Membrane Localization and Dynamics of Geranylgeranylated Rab5 Hypervariable Region

Eileen Edler[a], Eric Schulze[a,b], Matthias Stein[a*]

[a]Molecular Simulations and Design Group, Max Planck Institute for Dynamics of Complex Technical Systems, Sandtorstrasse 1, 39106 Magdeburg, Germany.

[b]International Max Planck Research School (IMPRS) for Advanced Methods in Process and Systems Engineering, Magdeburg, Germany.

*Corresponding author: Dr Matthias Stein, Molecular Simulations and Design Group, Max Planck Institute for Dynamics of Complex Technical Systems, Sandtorstrasse 1, 39106 Magdeburg, Germany. Email Matthias.stein@mpi-magdeburg.mpg.de, fax +49 391 6110 436.

Supplementary material

1 Parameters of a geranylgeranyl (GG) chain in all-atom simulations

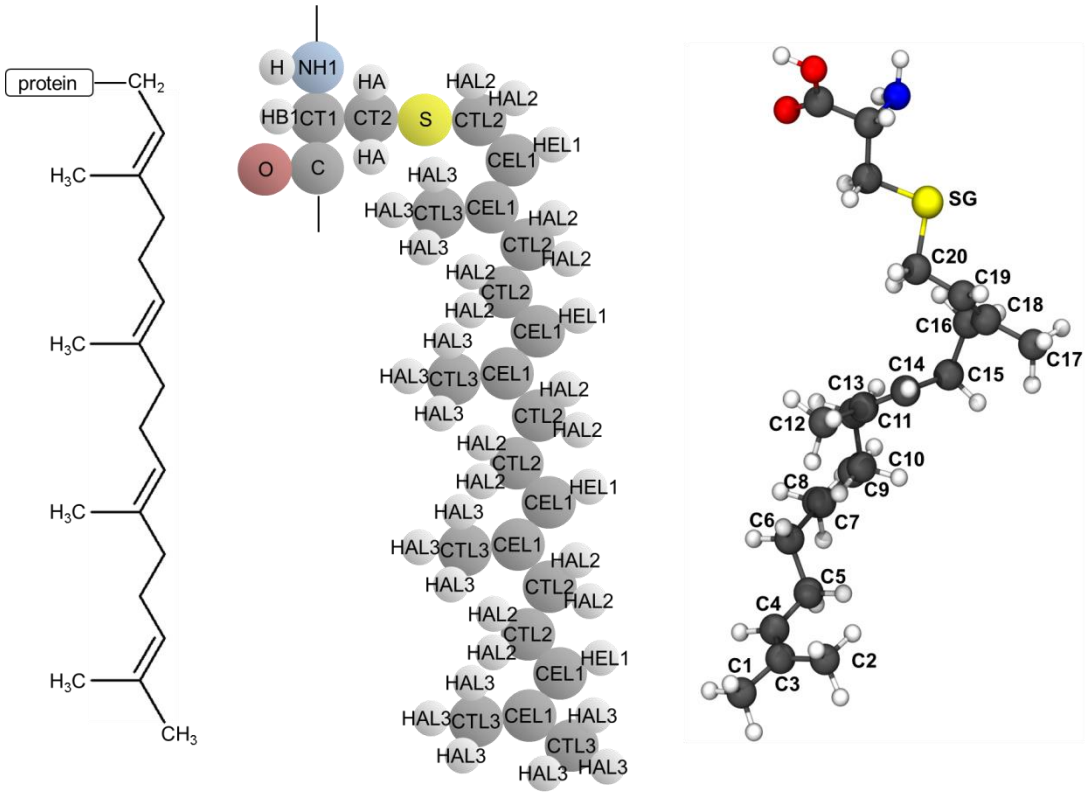

Figure S1 Structure of the CysGG residue in all-atom MD simulations. Atom names correspond to the nomenclature of the CHARMM36 protein (1) and lipid (2) force fields.

Table S1 Parameters for the GG chains taken from the all-atom CHARMM36 force fields for proteins and lipids; ((a) = CHARMM36 all-hydrogen parameter file for proteins, (b) = CHARMM36 all-hydrogen lipid parameter file).

	Force field parameters	remarks
Bond lengths	$V_{bond} = k_b(b - b_0)^2$	k_b:kcal·mol^{-1}·Å^{-2} b_0: Å
S-CTL2	k_b = 198.0; b_0 = 1.818	Corresponds to S-CT2 in (a) (1)
HA-CT2	k_b = 309.0; b_0 = 1.111	Corresponds to HA2-CT2 in (a) (1)
Bond angles:	$V_{angle} = k_\theta(\theta - \theta_0)^2$ $V_{Urey-Bradley} = k_{ub}(S - S_0)^2$	k_θ:kcal·mol^{-1}·rad^{-2} θ_0: degrees k_{ub}:kcal·mol^{-1}·Å^{-2} S_0: Å
CT2-S-CTL2	k_θ = 34.0; θ_0 = 95.0	Corresponds to CT3–S-CT2 (MET) in (a) (1)
S-CTL2-HAL2	k_θ = 46.1; θ_0 = 111.3	Corresponds to S-CT2-HA (CYS) in (a) (1)
S-CTL2-CEL1	k_θ = 58.0; θ_0 = 114.5	Corresponds to S-CT2-CT2 in (a) (1)
CTL3-CEL1-CTL3	k_θ = 22.0; θ_0 = 117.0	Corresponds to HEL1-CEL1-CTL3 in (b) (3)
CTL2-CEL1-CTL3	k_θ = 22.0; θ_0 = 117.0	Corresponds to HEL1-CEL1-CTL3 in (b) (3)
HA-CT2-CT1	k_θ = 26.5; θ_0 = 110.1 k_{ub} = 22.53; S_0 = 2.179	Corresponds to HA2-CT2-CT1 in (a) (1)
HA-CT2-HA	k_θ = 35.5; θ_0 = 109.0 k_{ub} = 5.40; S_0 = 1.802	Corresponds to HA2-CT2-HA2 in (a) (1)
S-CT2-HA	k_θ = 46.1; θ_0 = 111.3	Corresponds to S-CT2-HA2 in (a) (1)
Torsion angles:	$V_{dihedral} = k_\phi(1 + \cos(n\phi - \delta))$	k_ϕ:kcal·mol^{-1} n: - δ: degrees
HAL2-CTL2-S-CT2	k_ϕ = 0.28; n = 3; δ = 0.0	Corresponds to HA2-CT2-S-CT3 in (a) (1)
CEL1-CTL2-S-CT2	k_ϕ = -0.10; n = 3; δ = 0.0	Corresponds to X-CT2-OS-X in (a) (1)
HA-CT2-S-CTL2	k_ϕ = 0.28; n = 3; δ = 0.0	Corresponds to HA2-CT2-S-CT3 in (a) (1)
CTL2-S-CT2-CT1	I) k_ϕ = 0.24; n = 1; δ = 0.0 II) k_ϕ = 0.15; n = 2; δ = 0.0 III) k_ϕ = 0.27; n = 3; δ = 0.0	Corresponds to HS-S-CT2-CT3 in (a) (1)
HEL1-CEL1-CTL2-S	k_ϕ = 0.12; n = 3; δ = 0.0	Corresponds to HEL1-CEL1-CTL2-CTL2 in (b) (3)
CEL1-CEL1-CTL2-S	I) k_ϕ = 0.50; n = 1; δ = 180.0 II) k_ϕ = 1.30; n = 3; δ = 180.0	Corresponds to CEL2-CEL1-CTL2-CTL2 in (b) (3)
CTL3-CEL1-CTL3-HAL3	k_ϕ = 0.00; n = 3; δ = 0.0	Corresponds to HEL1-CEL1-CTL3-HAL3 in (b) (3)
CTL2-CEL1-CTL3-HAL3	k_ϕ = 0.00; n = 3; δ = 0.0	Corresponds to HEL1-CEL1-CTL3-HAL3 in (b) (3)
CTL3-CEL1-CTL2-CTL2	k_ϕ = 0.12; n = 3; δ = 0.0	Corresponds to HEL1-CEL1-CTL2-CTL2 in (b) (3)
CTL3-CEL1-CTL2-HAL2	k_ϕ = 0.00; n = 3; δ = 0.0	Corresponds to HEL1-CEL1-CTL2-HAL2 in (b) (3)

Table S2 Bond lengths between S and C backbone atoms of the GG chains as measured from quantum mechanical DFT calculations and compared to MD simulations.

	DFT (def2-SVP, BP86, ε=2)	MD, averaged over 3x 200ns	Deviation from QM calculation
	Bond length / nm	Bond length / nm	Deviation / nm
SG-C20	0.1858	0.1821 (± 0.0040)	-0.0037
C20-C19	0.1501	0.1510 (± 0.0029)	0.0009
C19=C18	0.1359	0.1349 (± 0.0027)	-0.0010
C18-C17	0.1511	0.1508 (± 0.0029)	-0.0004
C18-C16	0.1517	0.1512 (± 0.0029)	-0.0005
C16-C15	0.1555	0.1552 (± 0.0033)	-0.0003
C15-C14	0.1505	0.1513 (± 0.0030)	0.0007
C14=C13	0.1358	0.1349 (± 0.0027)	-0.0009
C13-C12	0.1512	0.1508 (± 0.0029)	-0.0004
C13-C11	0.1518	0.1513 (± 0.0029)	-0.0005
C11-C10	0.1554	0.1552 (± 0.0033)	-0.0001
C10-C9	0.1505	0.1513 (± 0.0029)	0.0008
C9=C8	0.1357	0.1349 (± 0.0027)	-0.0008
C8-C7	0.1512	0.1508 (± 0.0029)	-0.0004
C8-C6	0.1518	0.1513 (± 0.0029)	-0.0005
C6-C5	0.1554	0.1553 (± 0.0033)	-0.0001
C5-C4	0.1505	0.1513 (± 0.0030)	0.0008
C4=C3	0.1357	0.1347 (± 0.0027)	-0.0010
C3-C2	0.1511	0.1506 (± 0.0029)	-0.0004
C3-C1	0.1512	0.1505 (± 0.0029)	-0.0007

Table S3 Comparison of bond angles between C backbone atoms of GG chains in QM and MD calculations.

	DFT (def2-SVP, BP86, ε=2)	MD, averaged over 3x 200ns	Deviation from QM calculation
	Bond angle / °	Bond angle / °	Deviation / °
SG-C20-C19	109.0	112.5 (± 3.8)	3.5
C20-C19=C18	126.5	127.6 (± 3.2)	1.1
C19=C18-C17	120.6	121.4 (± 3.5)	0.9
C19=C18-C16	123.5	125.6 (± 3.3)	2.1
C17-C18-C16	115.9	112.5 (± 3.9)	-3.5
C18-C16-C15	114.9	114.1 (± 4.2)	-0.9
C16-C15-C14	113.9	112.4 (± 4.3)	-1.5
C15-C14=C13	128.0	127.3 (± 3.3)	-0.7
C14=C13-C12	120.8	121.4 (± 3.5)	0.6
C14=C13-C11	123.8	125.5 (± 3.2)	1.7
C12-C13-C11	115.4	112.5 (± 3.9)	-2.8
C13-C11-C10	113.6	114.0 (± 4.2)	0.5
C11-C10-C9	112.9	112.5 (± 4.2)	-0.4
C10-C9=C8	128.3	127.3 (± 3.3)	-1.1
C9=C8-C7	120.8	122.0 (± 3.7)	1.3
C9=C8-C6	123.8	125.2 (± 3.4)	1.4
C7-C8-C6	115.5	112.3 (± 3.9)	-3.2
C8-C6-C5	113.6	114.5 (± 4.4)	0.9
C6-C5-C4	112.9	112.5 (± 4.3)	-0.4
C5-C4=C3	128.5	127.0 (± 3.3)	-1.5
C4=C3-C2	124.5	125.6 (± 3.4)	1.1
C4=C3-C1	120.8	122.4 (± 3.6)	1.7
C2-C3-C1	114.7	111.3 (± 4.0)	-3.3

Table S4 Average torsion angles in MD simulations adopt values from multiple Gaussian distributions.

	MD, averaged over 3x 200ns			
	Torsion angle / °			
SG-C20-C19=C18	-119.9	119.5		
C20-C19=C18-C17	-180.0	180.0		
C20-C19=C18-C16	0.0			
C19=C18-C16-C15	-95.2	94.3		
C17-C18-C16-C15	-86.8	85.9		
C18-C16-C15-C14	-180.0	-70.3	69.7	180.0
C16-C15-C14=C13	-113.8	112.8		
C15-C14=C13-C12	-180.0	180.0		
C15-C14=C13-C11	-0.1			
C14=C13-C11-C10	-95.7	96.7		
C12-C13-C11-C10	-84.5	85.4		
C13-C11-C10-C9	-180.0	-69.8	70.5	180.0
C11-C10-C9=C8	-111.6	111.3		
C10-C9=C8-C7	-180.0	0.1	180.0	
C10-C9=C8-C6	-180.0	-0.1	180.0	
C9=C8-C6-C5	-96.2	0.6	96.3	
C7-C8-C6-C5	-180.0	-84.8	85.0	180.0
C8-C6-C5-C4		-71.1	70.3	
C6-C5-C4=C3	-101.8	98.2		
C5-C4=C3-C2	0.0			
C5-C4=C3-C1	-180.0	180.0		

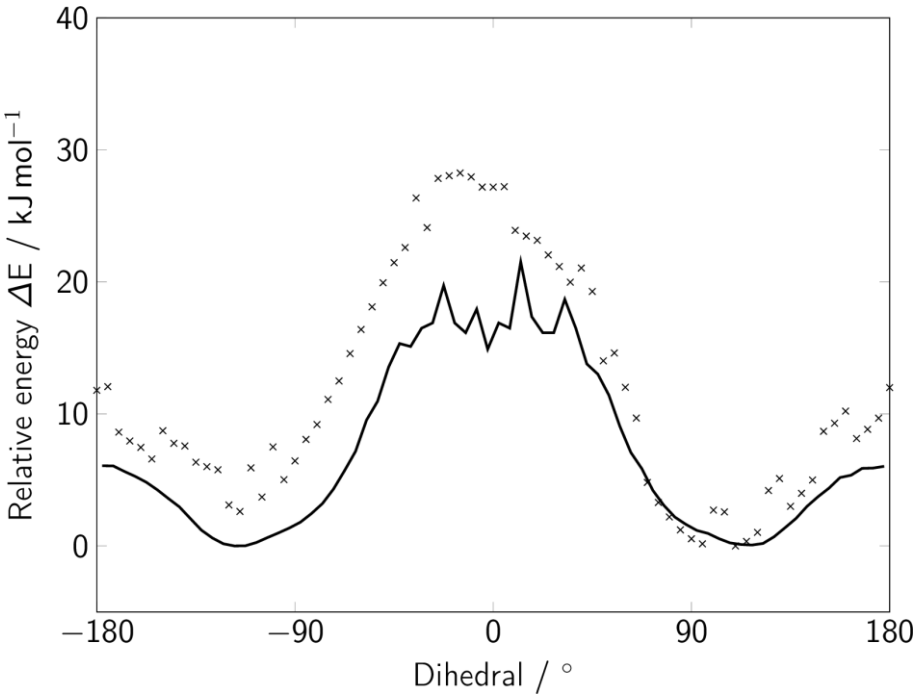

Figure S2 QM free energy torsional profile (crosses) and free energy torsional surface from the MD trajectories (solid line) around the ϕ(CEL1-CEL1-CTL2-CTL2) dihedral.

2 GG anchor parameters for MARTINI CG simulations

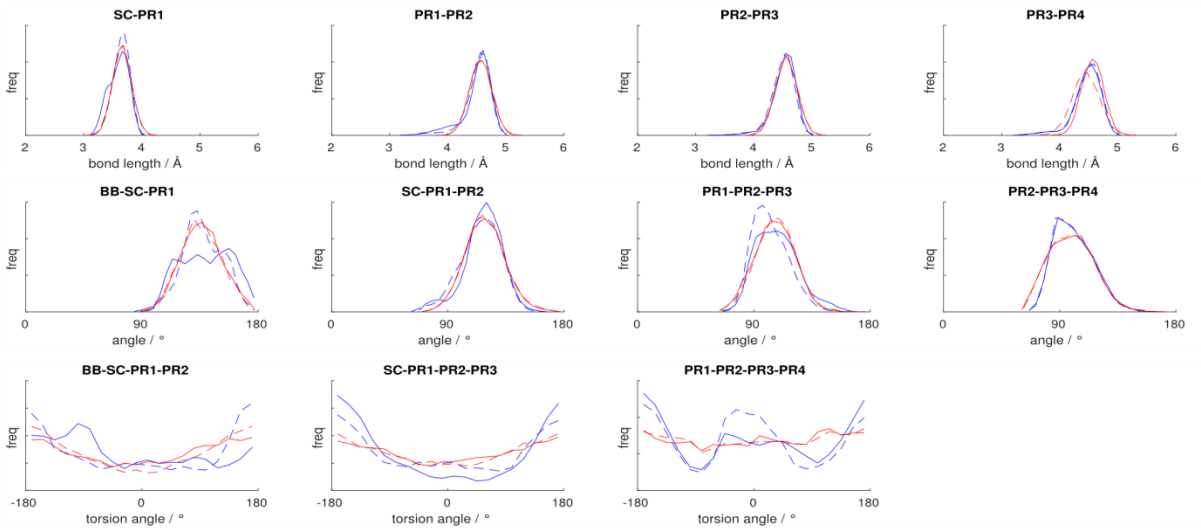

Figure S3 Comparison of bonded parameters in all-atom (blue) and coarse-grained (red) simulations. Both residues are shown individually: Cys^{212} (solid), Cys^{213} (dashed).

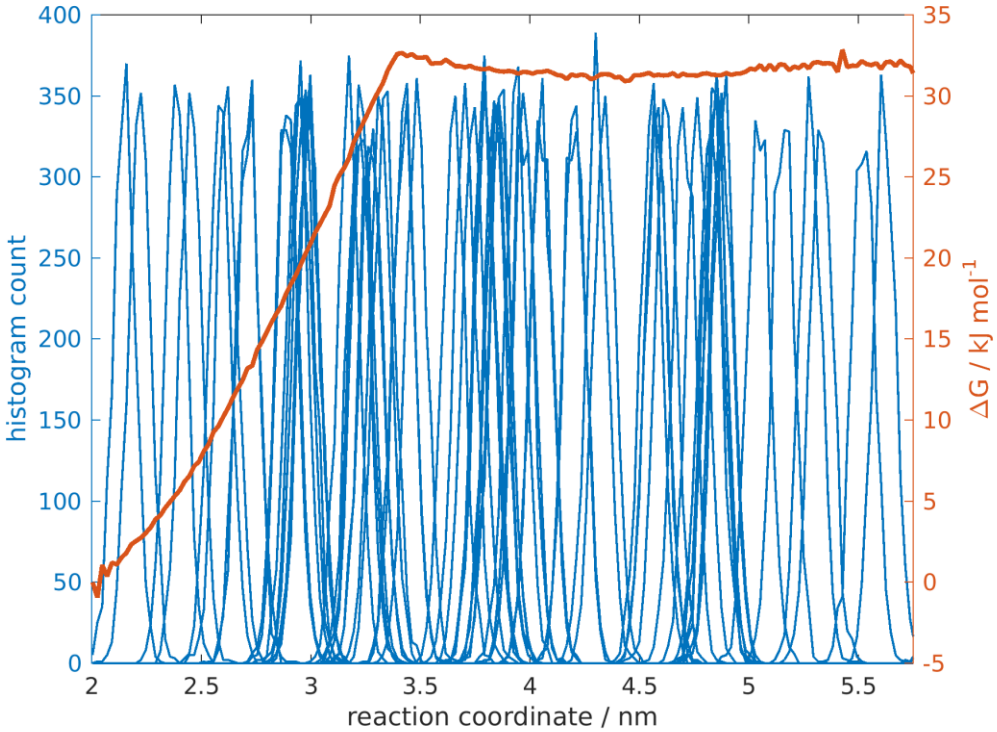

Figure S4 Umbrella sampling histograms (blue, left axis) and estimated free energy difference of the coarse-grained GG anchor water-to-bilayer transfer (orange, right axis). The reaction coordinate is the z-dimensional center-of-mass distance between bilayer and geranylgeranylated peptide

3 Membrane properties

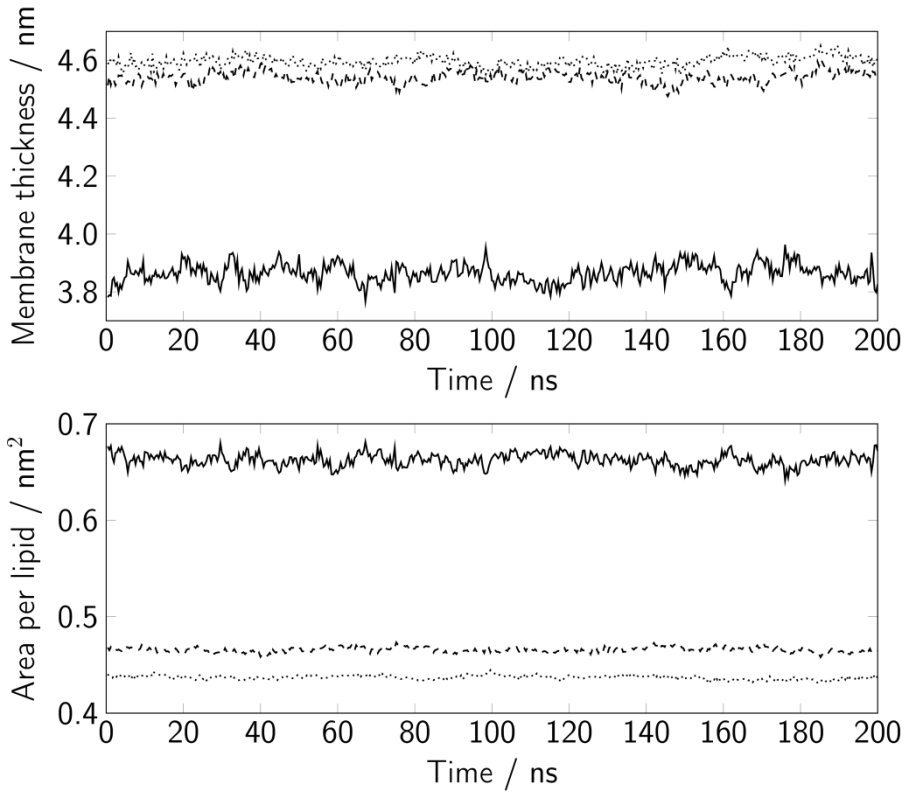

Figure S5 Global properties of the three membrane systems over 200 ns simulations. The membrane thickness (upper panel) as well as the area per lipid (lower panel) are shown for pure POPC (solid line), the ternary membrane (dotted line) as well as the six-component membrane (dashed line).

Table S5 Time-averaged membrane thickness and lipid area of the three different membrane systems for the whole membrane as well as in close proximity to the HVR$^{206\text{-}215}$ (cutoff radius 0.5 nm).

	Membrane system		
	Pure POPC	**Ternary**	**Six-component**
Global			
Thickness / nm	3.886	4.593	4.566
Lipid area / nm^2	0.661	0.466	0.499
Order parameter -S_{CD}	0.176	0.327	0.305
Local			
Thickness / nm	3.855	4.521	4.485
Lipid area / nm^2	0.628	0.422	0.485
Order parameter -S_{CD}	0.153	0.304	0.270
Without HVR			
Thickness / nm	3.893	4.604	4.546
Lipid area / nm^2	0.648	0.433	0.462

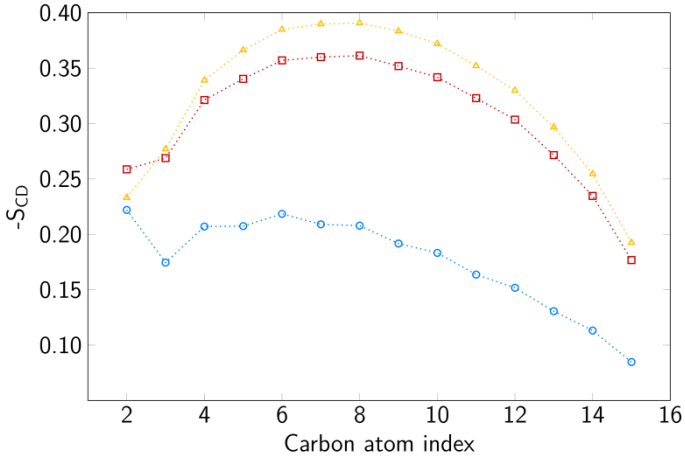

Figure S6 Order parameter -S_{CD} for the *sn-1* palmitoyl chains of pure POPC (blue), POPC and PSM in the ternary membrane (yellow) and POPC, PSM, POPE, POPS in the six-component membrane (red) as a function of the carbon atom.

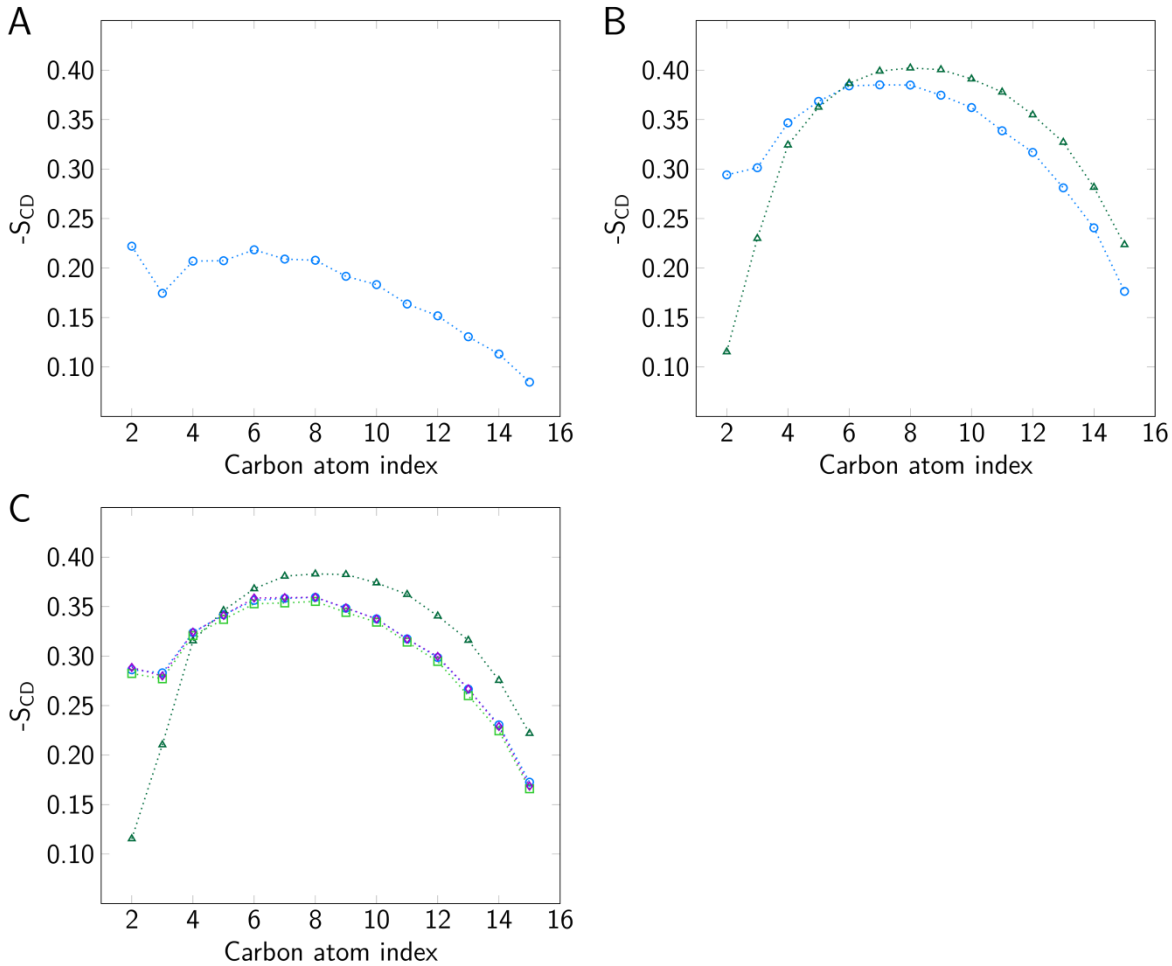

Figure S7 Order parameter -S_{CD} for different phospholipids for the three membrane systems; **A)** pure POPC, **B)** ternary mixture, and **C)** six-component membrane. The *sn-1* palmitoyl segments are shown for POPC (blue circles), PSM (green triangles), POPE (light green squares), and POPS (violet diamonds).

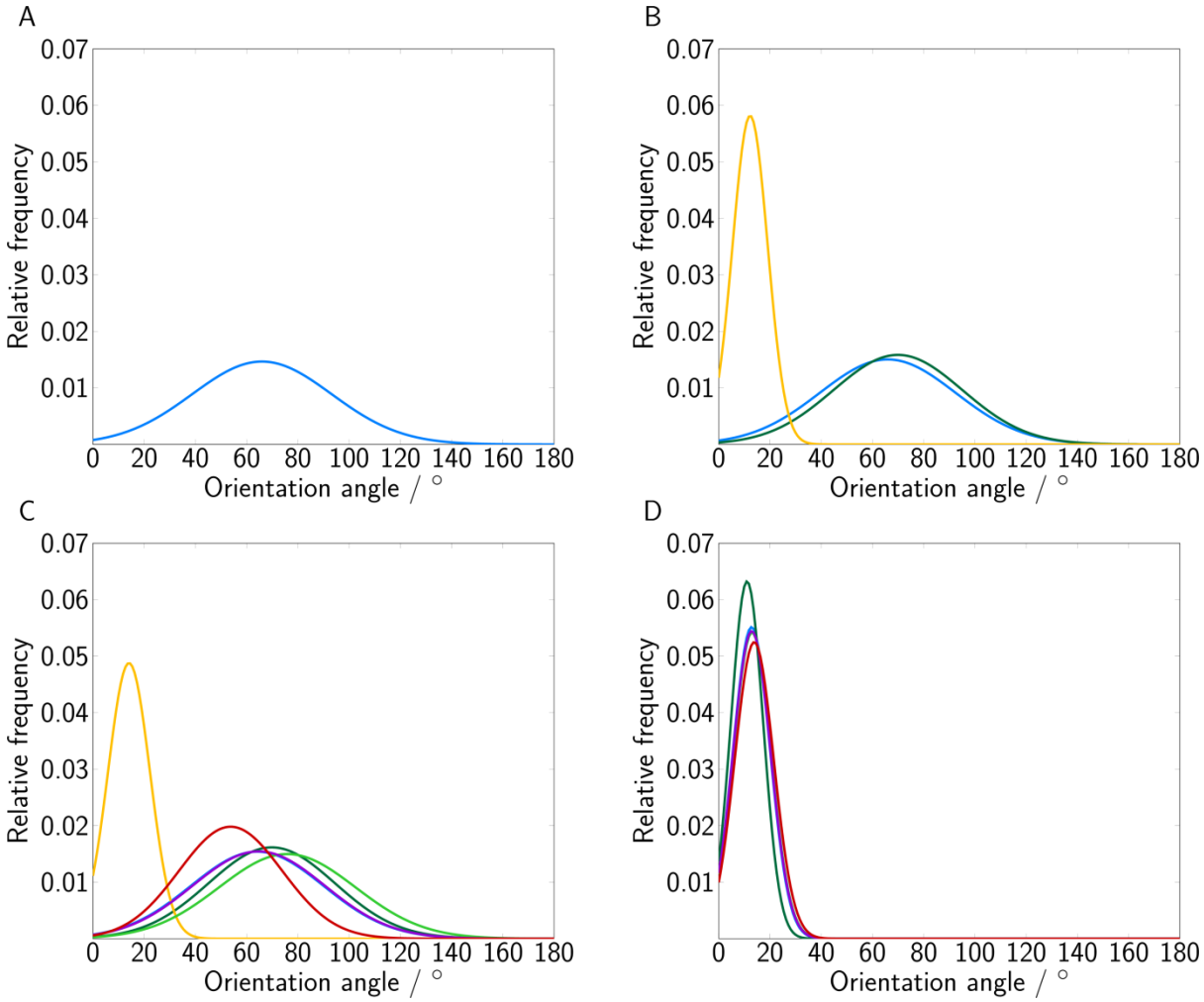

Figure S8 Distributions of lipid head group orientations in **A)** pure POPC, **B)** the ternary mixture, and **C)** the six-component membrane. **D)** Tail orientations of the phospholipids in the charged six-component membrane. Data are shown for POPC (blue), PSM (dark green), POPE (bright green), POPS (violet), the tilt angle of cholesterol rings (yellow), and the inositol ring angle of PI(3)P (red).

4 GG Anchor and HVR$^{206-215}$ properties

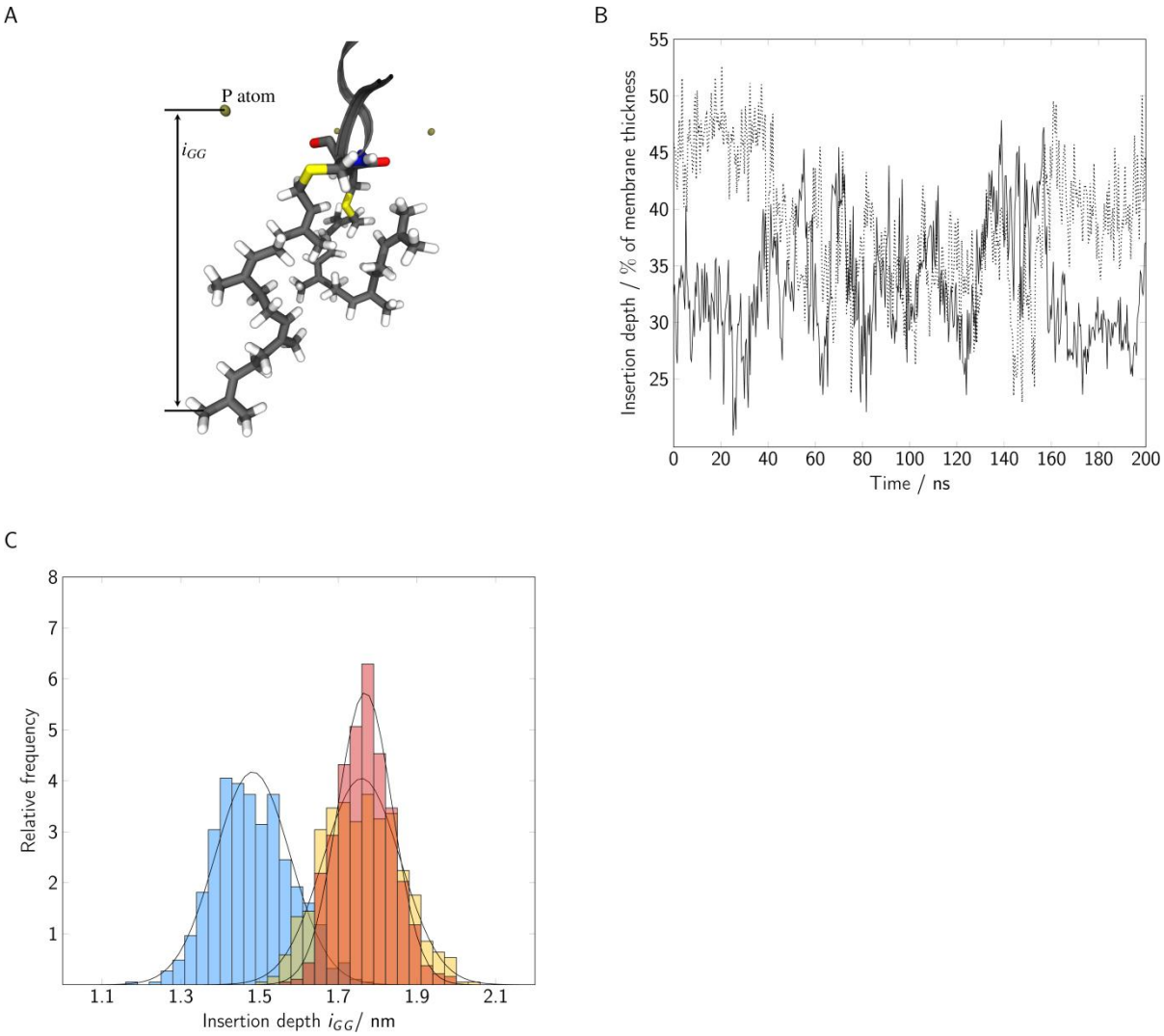

Figure S9 A) The GG insertion depth and the HVR end-to-end distance were defined as two variables describing the HVR structure. **B)** The insertion depth of one GG chain (solid line) is correlated with the movements of the other chain (dotted line), leaving at least one chain deeply inserted within the bilayer whereas the other one is allowed to bend. **C)** The GG insertion depth depends on the membrane system thickness; pure POPC (blue), uncharged ternary membrane (yellow), six-component membrane (red).

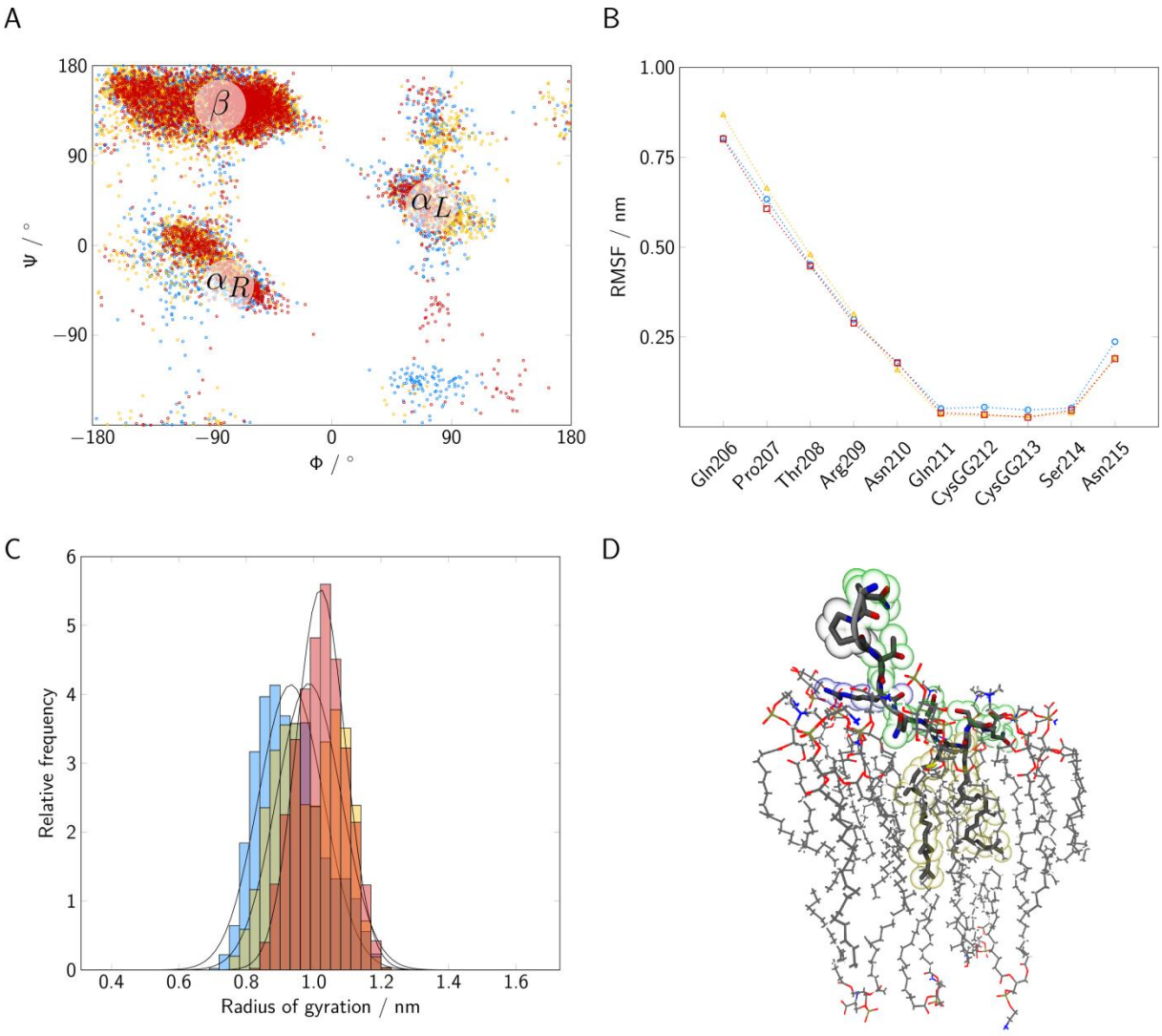

Figure S10 A) The averaged backbone torsion angles Φ and Ψ of the six HVR$^{206\text{-}215}$ replicates are represented in a Ramachandran plot with data from the POPC membrane shown in blue, from the ternary mixture in yellow and the six-component membrane in red. **B)** Root Mean Square Fluctuation (RMSF) of the HVR backbone C-alpha atoms is shown for the different membrane systems (colors as above). **C)** The radius of gyration is a measure for the HVR flexibility at the different model membranes. **D)** Peptide-lipid interactions in the six-component membrane with spheres of the polar residues colored in green, the non-polar proline in black, the basic arginine in blue and the GG chains in yellow.

Table S 6 Properties of the individual HVR$^{206-215}$ replicates in the three model membranes

Property	HVR 1	HVR 2	HVR 3	HVR 4	HVR 5	HVR 6
Pure POPC membrane						
GG insertion depth / nm	1.438	1.343	1.444	1.579	1.393	1.699
Radius of gyration / nm	0.959	0.895	0.913	0.890	0.864	1.072
Diffusion coefficient / 10^{-7} cm^{2}s^{-1}	0.69	1.02	0.83	0.80	0.62	0.71
Local thickness (c_r = 0.5 nm) / nm	3.846	3.808	3.842	3.892	3.879	3.864
Local order - S_{CD} (c_r = 0.5 nm)	0.160	0.143	0.161	0.135	0.159	0.161
Ternary membrane						
Surrounding lipids (c_r = 0.5 nm)						
POPC / %	41.1	25.4	35.0	44.2	35.8	35.4
CHOL / %	45.6	52.7	46.0	34.6	49.1	39.3
PSM / %	13.3	21.9	19.0	21.2	15.1	25.3
GG insertion depth / nm	1.746	2.130	1.610	1.818	1.448	1.803
Radius of gyration / nm	0.922	1.085	0.854	1.021	0.956	1.075
Diffusion coefficient / 10^{-7} cm^{2}s^{-1}	0.35	0.43	0.43	0.66	0.49	0.48
Local thickness (c_r = 0.5 nm) / nm	4.518	4.487	4.522	4.489	4.585	4.525
Local order - S_{CD} (c_r = 0.5 nm)	0.314	0.316	0.321	0.286	0.292	0.293
6-component membrane						
Surrounding lipids (c_r = 0.5 nm)						
POPC / %	28.4	7.0	15.8	16.1	4.4	16.9
CHOL / %	27.4	35.0	30.6	21.8	33.5	21.0
PSM / %	7.3	9.1	18.3	14.8	12.3	10.6
POPE / %	17.7	30.3	22.0	29.1	29.9	29.7
POPS / %	7.2	13.4	11.1	10.8	14.0	12.4
PI(3)P / %	12.0	5.2	2.2	7.4	5.9	9.4
GG insertion depth / nm	1.861	1.682	1.941	1.617	1.744	1.765
Radius of gyration / nm	1.038	0.981	1.059	0.940	1.013	1.090
Diffusion coefficient / 10^{-7} cm^{2}s^{-1}	0.36	0.57	0.39	0.45	0.35	0.49
Local thickness (c_r = 0.5 nm) / nm	4.525	4.480	4.465	4.454	4.488	4.500
Local order - S_{CD} (c_r = 0.5 nm)	0.297	0.281	0.262	0.261	0.256	0.263

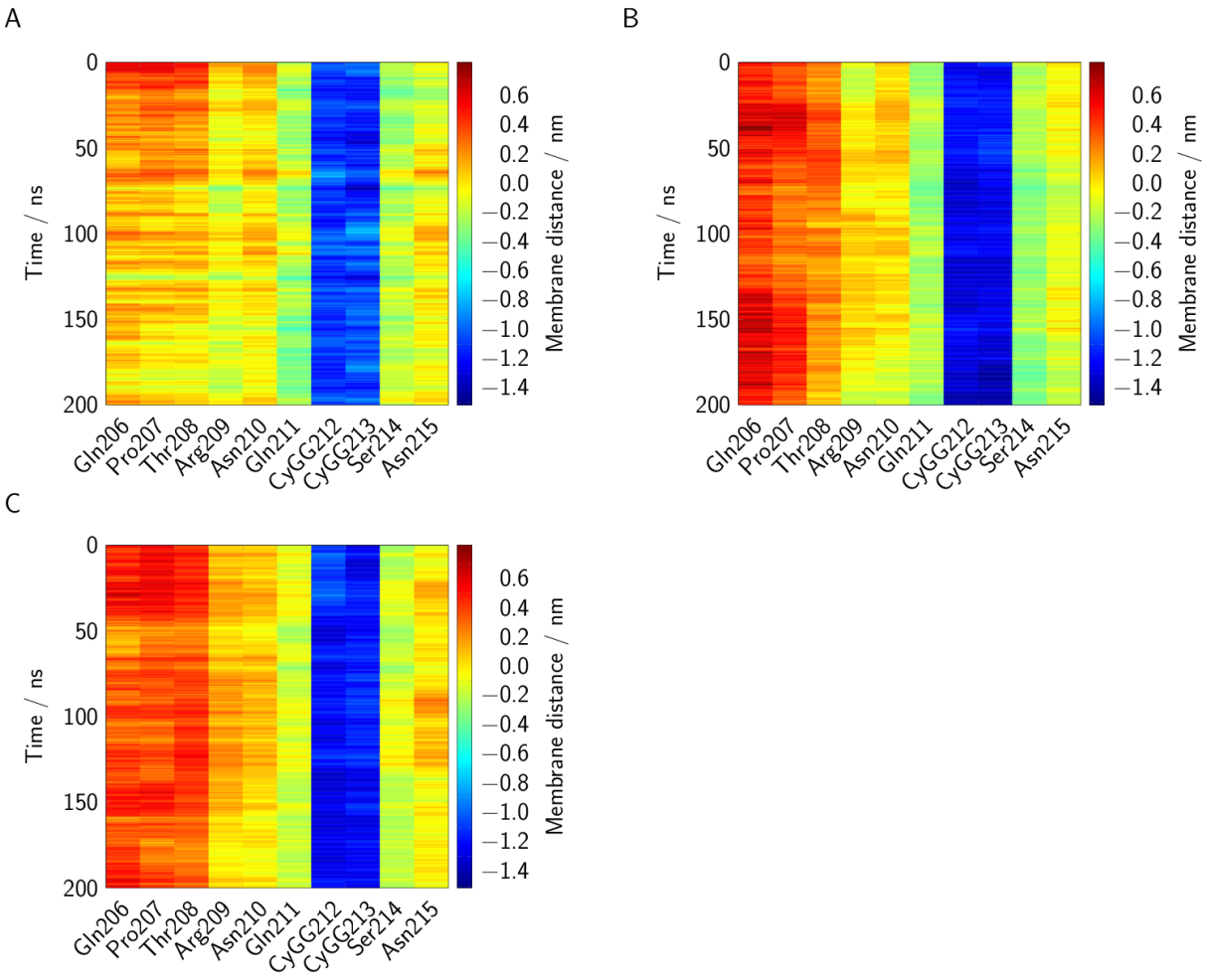

Figure S11 Average change of the amino acid-membrane distances of the six $HVR^{206-215}$ replicates over 200 ns in **A)** pure POPC, **B)** the ternary mixture and **C)** the six-component membrane.

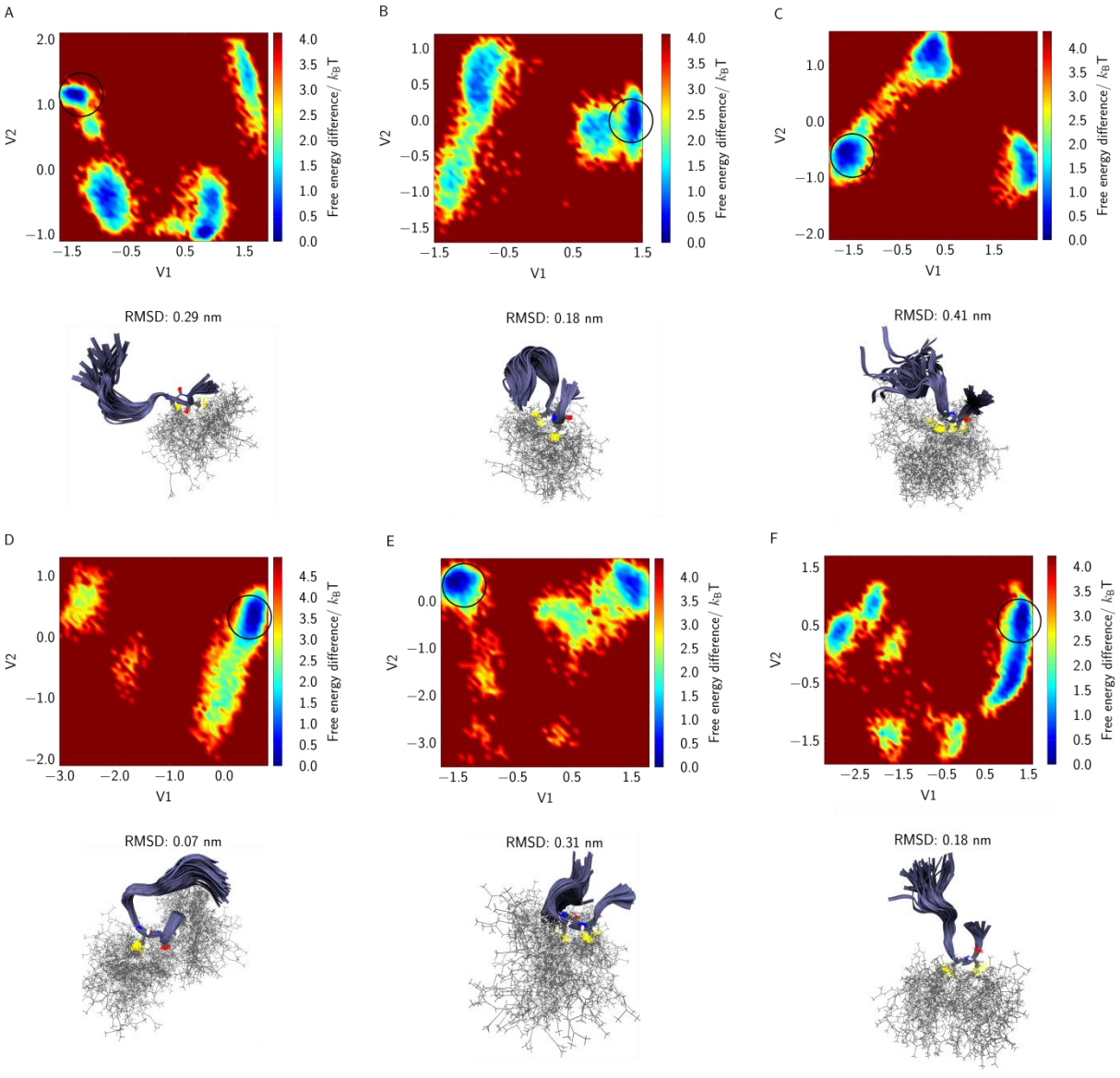

Figure S12 Dihedral PCA free energy landscapes of the truncated Rab5 HVR$^{206\text{-}215}$ (**A-F**, six individual HVR replicates) in a pure POPC bilayer plotted as a function of the first two principal components (V1 and V2). Structures corresponding to the lowest energy well are shown below; the RMSD was measured for the structures belonging to one minimum energy conformation.

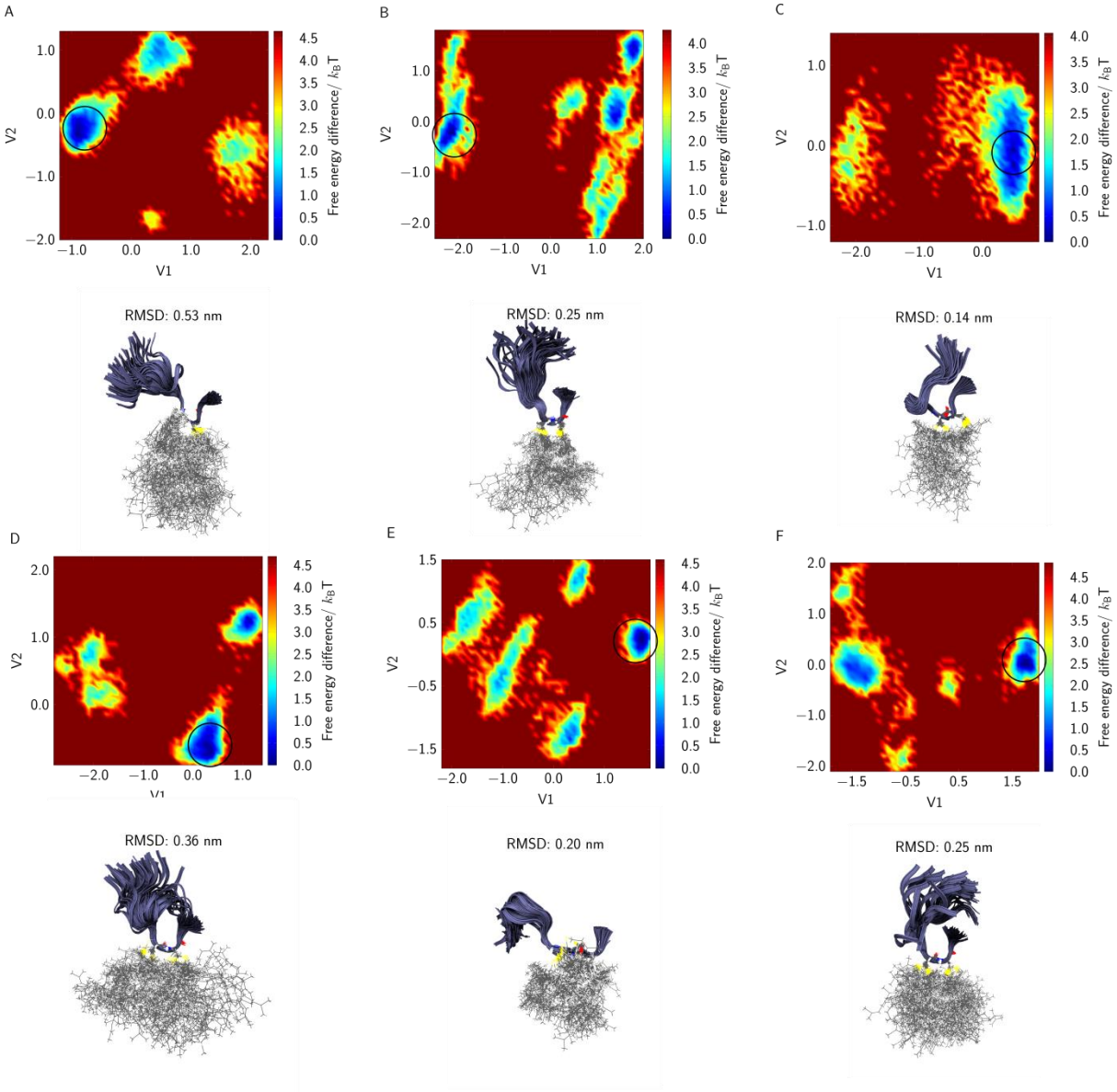

Figure S13 Dihedral PCA free energy landscapes of the truncated Rab5 HVR$^{206\text{-}215}$ (**A-F**, six individual HVR replicates) in the ternary membrane plotted as a function of the first two principal components (V1 and V2). The lowest energy structures are shown below; the RMSD was measured for the structures belonging to one minimum energy conformation.

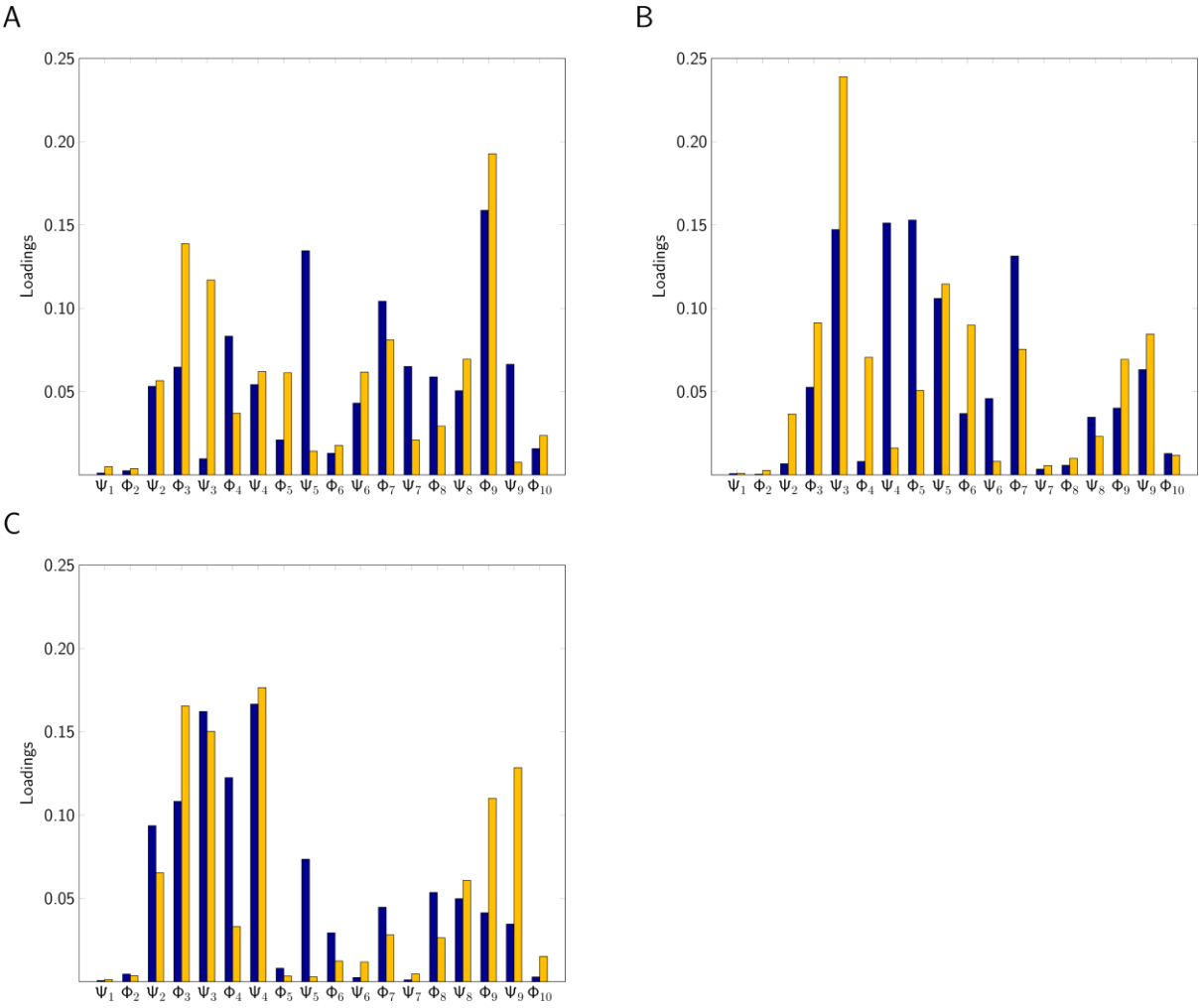

Figure S14 Impact of the dihedral angles of the HVR$^{206\text{-}215}$ on principal components V1 (blue) and V2 (yellow). The loadings are the coefficients of the linear combinations of the sin- and cos-transformed angles generating the first two principal components. Data are shown for **A)** pure POPC, **B)** the ternary mixture and **C)** the six-component membrane.

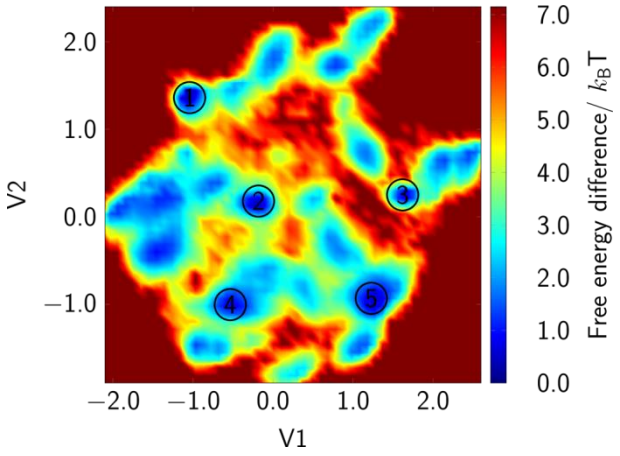

Figure S15 Dihedral PCA free energy landscapes of the truncated Rab5 HVR$^{206\text{-}215}$ replicates in all investigated membrane systems plotted as a function of the first two principal components (V1 and V2). The structures corresponding to the energy minima (1-5) were at no time present in only one membrane type indicating a sufficient sampling of the peptide.

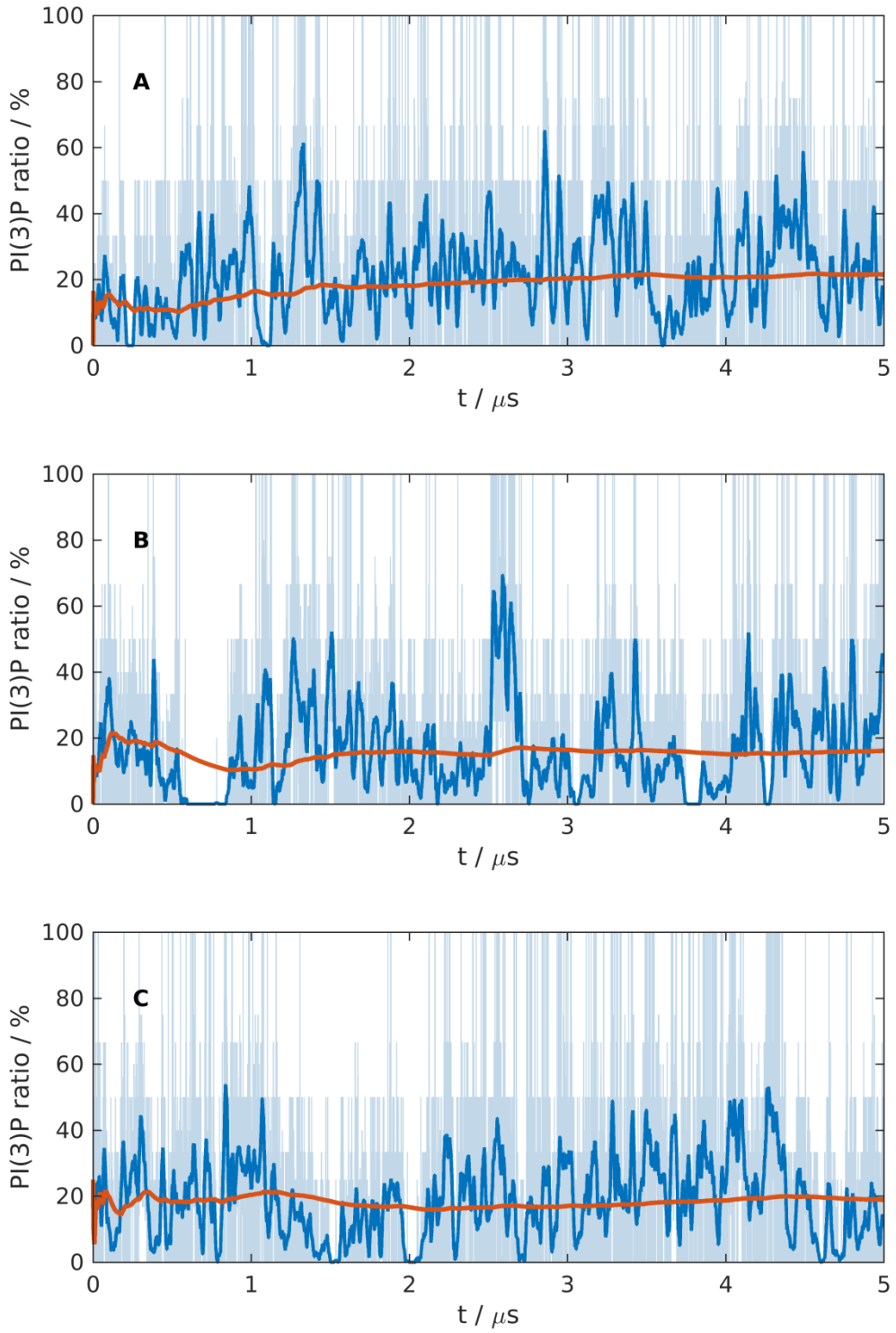

Figure S16 PI(3)P fraction within a sphere of 1 nm radius centered on the center of mass of the sulfur beads of the peptide plotted versus the simulation time. Light blue: raw data; dark blue: moving average of 50 ns; red: total average from t=0 to t. **A), B)** and **C)** represent independent replicates with different initial configurations. The bilayer composition is the one of the six-component bilayer.

Table S7 Initial configurations of the CG enrichment simulations for three independent replicates. Presented is the absolute number of lipids within a distance cutoff of 1 nm and 1.5 nm.

	Replicate A		***Replicate B***		***Replicate C***	
Lipid	**1 nm**	**1.5 nm**	**1 nm**	**1.5 nm**	**1 nm**	**1.5 nm**
CHOL	2	6	3	4	1	4
PI(3)P	0	1	0	1	1	2
PSM	0	1	1	1	0	0
POPE	1	3	2	4	2	7
POPS	0	1	0	0	0	0
POPC	2	2	0	5	0	0

Supplementary references

1. Best, R. B., X. Zhu, J. Shim, P. E. M. Lopes, J. Mittal, M. Feig, and A. D. MacKerell. 2012. Optimization of the Additive CHARMM All-Atom Protein Force Field Targeting Improved Sampling of the Backbone phi, psi and Side-Chain chi(1) and chi(2) Dihedral Angles. J. Chem. Theory Comput. 8:3257-3273.
2. Pastor, R. W., and A. D. MacKerell. 2011. Development of the CHARMM Force Field for Lipids. J. Phys. Chem. Lett. 2:1526-1532.
3. Klauda, J. B., R. M. Venable, J. A. Freites, J. W. O'Connor, D. J. Tobias, C. Mondragon-Ramirez, I. Vorobyov, A. D. MacKerell, and R. W. Pastor. 2010. Update of the CHARMM All-Atom Additive Force Field for Lipids: Validation on Six Lipid Types. J. Phys. Chem. B 114:7830-7843.